Tuning Negative Capacitance in PbZr$_{0.2}$Ti$_{0.8}$O$_3$/SrTiO$_3$ Heterostructures via Layer Thickness Ratio

Yifei Hao[1,2,†] Tianlin Li[1,2,†] Yu Yun,[1,2] Xin Li,[1,2] Xuegang Chen,[1,2] Jingfeng Song[1,2]
Zahra Ahmadi,[2,3] Jeffrey E. Shield,[2,3] Xiaoshan Xu,[1,2] and Xia Hong[1,2,*]

[1]*Department of Physics & Astronomy, University of Nebraska-Lincoln, Lincoln, Nebraska 68588-0299, USA*

[2]*Nebraska Center for Materials and Nanoscience, University of Nebraska-Lincoln, Lincoln,
Nebraska 68588-0299, USA*

[3]*Department of Mechanical & Materials Engineering, University of Nebraska-Lincoln, Lincoln,
Nebraska 68588-0511, USA*

In this work, we exploit the ferroelectric-dielectric layer thickness ratio r as an effective tuning parameter to control the ferroelectric polarization and transient negative capacitance (NC) state in epitaxial PbZr$_{0.2}$Ti$_{0.8}$O$_3$/SrTiO$_3$ bilayer heterostructures. The remnant polarization decreases monotonically with decreasing r, with the system exhibiting an abrupt transition from ferroelectric to dielectric dominated behavior at a critical ratio r_c of 8 to 7, which is consistent with the evolution of the free-energy profile modeled via Landau theory. For samples with large r, the polarization switching dynamics during the transient NC regime can be well described by the nucleation and growth model, with the narrow distribution of the characteristic switching time (t_0) pointing to a domain-wall-motion-limited behavior. Right below r_c, we observe a significantly broadened distribution of t_0, which can be attributed to the emergence of a multidomain state. The transient NC mode is quenched in samples with $r < 6$, confirming that the ferroelectric order is suppressed. Our study provides critical information for optimizing the materials design for complex oxide-based NC transistors, paving the path for their application in low-power nanoelectronics.

I. INTRODUCTION

The negative capacitance (NC) effect in ferroelectrics has attracted extensive research interests recently as it can be exploited to construct steep-slope FETs [1,2], which provides a promising route to transcending the power-scaling crisis of the semiconductor technology in the post-Moore regime [3]. For single-layer ferroelectrics, the NC effect originates from the negative curvature of the ferroelectric (FE) free-energy double well. It can lead to a transient NC mode upon polarization (P) switching, which, however, cannot be directly exploited for steady-state operation of the FET devices [4]. To stabilize the steady-state NC mode, a conventional approach is to connect a dielectric (DE) layer with the FE gate in series to provide dielectric matching [5]. To date, a wide variety of material combinations have been investigated, with the ferroelectric candidates including the perovskite oxides [6,7], doped hafnium oxides [8], and van der Waals ferroelectrics [9]. Among them, the perovskite oxides have the distinct advantage that it is possible to combine structurally similar

oxide FE, DE, and conductive channel layers into epitaxial heterostructure form [10–12], which promises atomically sharp interfaces with low defect states [13].

Previous studies of the complex oxide heterostructures and superlattices have shown that the presence of the dielectric layer imposes a strong depolarization field, which effectively competes with the ferroelectric ordering energy, suppresses the ordering temperature, and even leads to formation of multidomain states [10–12,14]. However, the evolution of the free-energy landscape and polarization switching dynamics in the FE/DE stacks remains a highly contentious topic. Several dynamic models have been proposed, including the uniform polarization switching [4], domain nucleation and growth (NG) [15–19], and multidomain compact models [20–22]. The applicable condition of the Landau theory in describing the ferroelectric state and NC mode in these stack capacitors also calls for further examination [23]. A systematic study of the effect of materials design on the ferroelectric order and polarization dynamics is thus imperative for developing complex oxide-based NC FETs.

In this work, we report a comprehensive study of the switching hysteresis and transient NC mode in epitaxial heterostructures composed of ferroelectric PbZr$_{0.2}$Ti$_{0.8}$O$_3$

---

*xia.hong@unl.edu
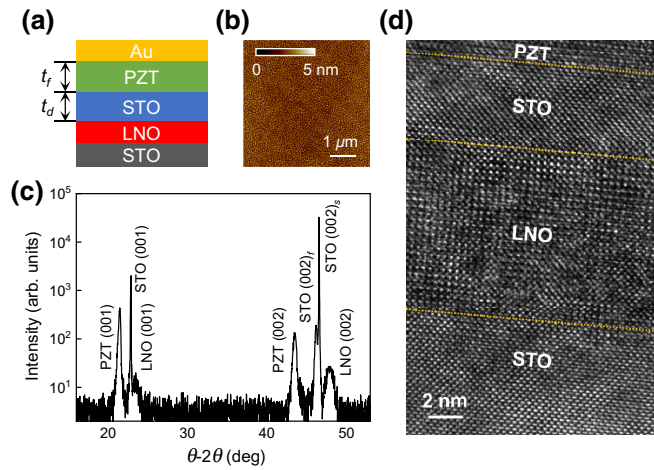†Y.H. and T.L. contributed equally to this work.

034004-1

FIG. 1. (a) Sample schematic. (b) AFM topography image and (c) XRD $\theta-2\theta$ scan taken on a 60 nm PZT/40 nm STO/10 nm LNO ($r = 1.5$) sample. STO $(002)_f$ and $(002)_s$ label the Bragg peaks of the STO film and substrate, respectively. The (001) peak for the STO film is close to the substrate peak and not resolved. (d) HRTEM image of a 100 nm PZT/5 nm STO/10 nm LNO ($r = 20$) sample. The dotted lines mark the interfaces.

(PZT) and dielectric SrTiO$_3$ (STO) bilayer thin films, with the thickness ratio between the FE (t_f) and DE (t_d) layers $r = t_f /t_d$ varying from 20 to 1 [Fig. 1(a)]. The remnant polarization (P_r) of the PZT/STO stack decreases monotonically with increasing STO content, with an abrupt suppression of P_r occurring at the critical value (r_c) of 8 to 7, which can be well described by Landau-theory modeling. By characterizing the transient NC mode in these samples, we confirm the gradually diminishing negative curvature in the free energy with decreasing r. Modeling the charge switching dynamics in the transient NC regime reveals switching characteristics dominated by domain-wall (DW) motion in samples with large r, which evolves to a nucleation-limited behavior in samples slightly below r_c, suggesting the emergence of a multidomain state. Our study provides critical information about the transition from a ferroelectric to dielectric dominated behavior in PZT/STO heterostructures, which can be utilized to optimize the materials design for their application in NC-based nanoelectronics.

II. SAMPLE PREPARATION AND CHARACTERIZATION

We deposit epitaxial PZT/STO bilayer heterostructures on 10-nm LaNiO$_3$ (LNO) buffered STO (001) substrates using off-axis radio-frequency magnetron sputtering. To ensure all samples have similar strain state, we keep the total thickness of the heterostructure to be about 100 nm (Supplemental Material) [24]. The PZT, LNO, and STO layers are deposited *in situ* subsequently at 500 °C, with the process gas of 120 mTorr (Ar:O$_2$=2:1), 60 mTorr

(Ar:O$_2$=1:2), and 60 mTorr (Ar:O$_2$=2:1), respectively. Atomic force microscopy (AFM) studies show that these samples possess smooth surface morphology, with a typical root-mean-square roughness of about 5 Å [Fig. 1(b)]. The high crystallinity of the samples is confirmed by XRD and HRTEM. Figure 1(c) shows the x-ray $\theta–2\theta$ scan taken on a 60 nm PZT/40 nm STO/10 nm LNO sample, which reveals (001) growth for all layers with no impurity phase observed. The c-axis lattice constants for LNO and STO are 3.81 and 3.93 Å, respectively. For all heterostructures, the c-axis lattice constant of PZT is 4.17 ± 0.1 Å, consistent with films strained on STO substrates [25], and does not show appreciable dependence on r [24], suggesting that all samples are in a similar strain state. As shown in the HRTEM image, the heterostructure possesses atomically sharp STO/LNO and PZT/STO interfaces [Fig. 1(d)]. We then fabricate the samples into capacitor devices by depositing an array of square electrodes (30 nm Au, width of 10–400 μm) on top of the heterostructures. The LNO layer serves as the bottom electrode for electrical measurements. The P-V and the C-V measurements are carried out in Lakeshore TTP4 probe station using Keithley 4200A-SCS Semiconductor Parameter Analyzer with model 4225-PMU I-V module. The transient switching measurements are taken using a functional generator (HP 33120A) and oscilloscope (Tektronix TBS 1052B).

III. FERROELECTRIC TO DIELECTRIC TRANSITION

We first characterize the dielectric and ferroelectric switching characteristics of the PZT/STO stacks with different thickness ratios. To measure the P-E loop, we apply a triangle wave of bias voltage (V_{bias}) to the capacitor. To compare results for samples with different r values, we define an effective electric field $E = V_{\text{bias}}/(t_f + t_d)$. The polarization is calculated by integrating the charging current (I) with respect to time t, $P(t) = \int_0^t I(t)dt/A$, where A is the capacitor area (Supplemental Material) [24]. As shown in Fig. 2(a), the single-layer PZT capacitor shows a robust switching hysteresis, with the remnant polarization (P_r) of about 78 μC cm^{-2} and coercive field of $+0.34/-0.26$ MV cm^{-1}, consistent with previously reported values [7,13]. The polarization asymmetry has been widely observed in epitaxial PZT thin films, which can be attributed to the asymmetric boundary condition [25,26]. For the PZT/STO stack capacitors, P_r decreases progressively with increasing content of STO. The switching field, in contrast, first increases in samples with large r values. This is understandable as only a fraction of V_{bias} is applied across the PZT layer. Compared with the P-E loop for PZT, there is a shoulderlike feature observed upon polarization switching for the $r = 20–7$ samples, which correlates with the double-peak feature in the switching current hysteresis (Supplemental Material) [24]. This
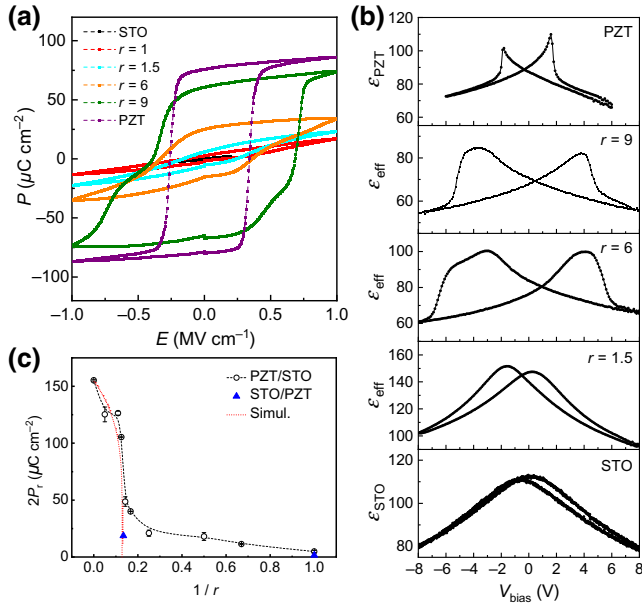
FIG. 2. (a) $P(E)$ hysteresis loops taken on PZT/STO stacks with different r. (b) Effective dielectric constant versus V_{bias} taken on 100 nm PZT, STO, and PZT/STO stack capacitors with different r. (c) $2P_r$ as a function of $1/r$ for PZT (open circle), PZT/STO (open circles), and STO/PZT (solid triangles). The red dashed line is the simulation result using the single-domain model.

feature can be attributed to the competition between two types of polarization switching kinematics: the nucleation and growth process with a much faster switching speed, and the emergence of a multidomain state accompanied with the slower DW propagation. Previous theoretical simulation has predicted this kind of feature for ferroelectric thin films with reduced thickness, where enhanced depolarization field leads to multidomain formation [22]. Around $r = 8$–7, there is a sudden drop of P_r, suggesting the suppressed ferroelectric order. It is worth noting that the switching hysteresis is not entirely quenched for the $r < r_c$ samples, which can be attributed to the fact that STO is an incipient ferroelectric [27–29]. Indeed, we observe a dielectriclike P-E response for single-layer STO at low bias ($V_{bias} = \pm 2$ V), which evolves to a finite P_r at $V_{bias} = \pm 10$ V (Supplemental Material) [24]. A similar suppression of P_r has been observed in the STO/PZT heterostructures [Fig. 2(c)], where we switch the growth sequence of the PZT and STO layers (Fig. S5 within the Supplemental Material) [24]. The further quenched P_r in STO/PZT can be attributed to the suppressed ferroelectric order in STO subjected to tensile strain on PZT [27]. As both systems exhibit similar FE-DE transition with increasing STO content, we focus our study on the PZT/STO system for their lower leakage.

The suppression of polarization switching is also observed in the C-V characteristics. We measure the C-V

curves of the samples at 100 kHz with 20 mV drive ac voltage. In Fig. 2(b), the capacitance of the stack capacitor is converted to the effective dielectric constant using $\varepsilon_{eff} = C[(t_f + t_d)/\varepsilon_0 A]$. The single-layer PZT film shows the typical butterfly shape of C-V for ferroelectrics. For the $r = 9$–6 samples, there is a broadening of the butterfly shape, which shares a similar origin with the shoulder feature in the P-E loop. The switching hysteresis is gradually diminished with decreasing r. The single-layer STO sample exhibits a dielectric behavior at low V_{bias} range, with ε_{STO} decreasing with bias field [30]. At zero bias, the dielectric constant of STO is around 118, which is in excellent agreement with that obtained from the low-field P-V_{bias} data (Fig. S6 within the Supplemental Material) [24] and within the range of previously reported values [10,27,31]. It is worth noting that ε_{eff} for the $r = 1$ and 1.5 PZT/STO stack capacitors is higher than those obtained on single-layer PZT (ε_{PZT}) and STO (ε_{STO}) [24], yielding strong evidence to the existence of the steady-state NC mode in the PZT layer, which can be attributed to the emergence of soft DWs in the multidomain state at high STO content [10].

Figure 2(c) plots $2P_r$ as a function of $1/r$. There is a sudden suppression of $2P_r$ at a critical thickness ratio r_c of 8 to 7, below which $2P_r$ shows only a moderate decrease. To gain a quantitative understanding of the abrupt change in P_r around r_c, we exploit Landau theory to model the evolution of free energy for the FE/DE stack capacitors. Assuming a homogenous single domain picture, the phenomenological formalism of Gibbs free-energy area density g_s as a function of polarization P is given by the Landau-Ginzburg-Devonshire (LGD) formula [5],

$$g_s(P,V) = t_f \left(\alpha P^2 + \beta P^4 + \gamma P^6 \right) + t_d \times \frac{P^2}{2\varepsilon_d \varepsilon_0} - PV. \tag{1}$$

Here the first term describes the free energy of the FE layer, where α, β, and γ are the Landau coefficients. The second term is the free energy associated with the DE layer, where ε_0 is the vacuum permittivity and $\varepsilon_d \approx 120$ for STO. The last term gives the electrostatic energy associated with the applied voltage V. By minimizing g_s at a given V, i.e., $\partial g_s / \partial P = 0$ and $\partial^2 g_s / \partial P^2 > 0$, we establish the relation between P and V:

$$V = t_f \left(2\alpha P + 4\beta P^3 + 6\gamma P^5 \right) + t_d \times \frac{P}{\varepsilon_d \varepsilon_0}. \tag{2}$$

Figure 3(a) shows the experimental P-E loops of the 100 nm PZT ($1/r \rightarrow 0$) measured at different frequencies. The coercive field E_c increases progressively with the measurement frequency f, while the spontaneous polarization remains unchanged. The E_c–f curve follows a
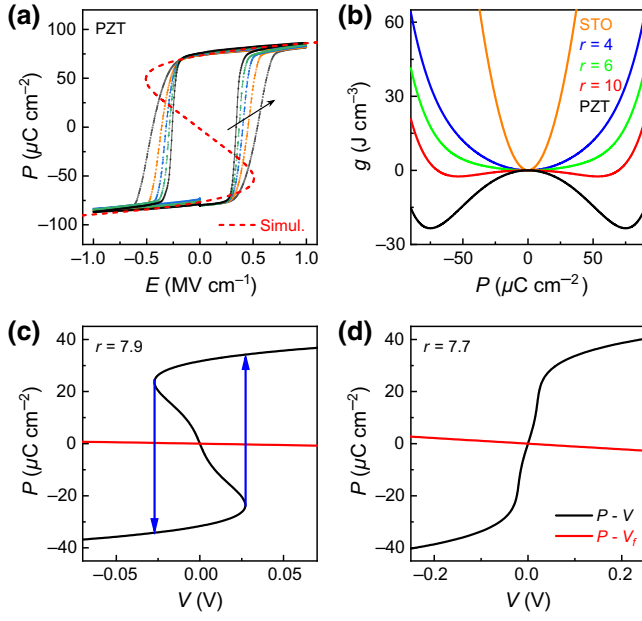
FIG. 3. (a) $P(E)$ hysteresis loops taken on a 100 nm PZT capacitor at 1, 2.5, 5, 10, and 25 kHz (along the arrow direction), superimposed with the simulated $P(E)$ (dashed line). (b) Simulated $g(P)$ for PZT/STO stacks with different r at zero bias. (c)–(d) Simulated polarization of PZT/STO stacks as a function of total voltage (V) and voltage across the FE layer (V_f) for (c) $r = 7.9$ and (d) 7.7. $t_{STO} = 10$ nm. The arrows in (c) illustrate the polarization switching as the free energy becomes unstable.

FIG. 4. (a) Voltage across the $r = 8$ stack capacitor (V_{cap}) during charging and discharging upon applied square wave source voltage (V_s). Inset: circuit schematic. Load resistor $R = 9.86$ kΩ. (b) Transient NC in samples with $r = 8$, 7, 6. (c)–(e) Q_s versus V_{cap} extracted for samples shown in (b).

clear power-law dependence (Supplemental Material) [24] similar to previous reports [32], indicating NG-dominated polarization switching. Fitting the data with Eq. (2) yields $\alpha = -6 \times 10^7$ m F^{-1}, $\beta = -9.1 \times 10^6$ m^5 C^{-2} F^{-1}, and $\gamma = 7.4 \times 10^7$ m^9 C^{-4} F^{-1}, which are close to the values reported in the literature [7]. This model well describes P_r of the sample. The measured E_c, on the other hand, is smaller than the simulation result, which is also a signature of DW motion-dominated behavior. Here $\beta < 0$ indicates that the transition from FE-DE is first order. We thus expect an abrupt change in $2P_r$ when r approaches the critical value at $r_c = [-2\alpha\varepsilon_d\varepsilon_0]^{-1} \approx 7.8$. Figure 2(c) shows the simulated r dependence of $2P_r$ using Eq. (2), which well describes the sudden suppressing of the polarization at $r = 8$–7.

Next, we simulate the free-energy profile of the DE-FE systems using Eq. (1) with the extracted Landau coefficients. As shown in Fig. 3(b), the free-energy density, $g = g_s/(t_d + t_f)$, evolves from the ferroelectric characteristic for large r to a dielectriclike behavior for small r. Close to r_c, the g-P relation transitions abruptly from a shallow double well to a broad single minimum. Such a change is clearly illustrated in the simulated P-V switching characteristics. For both $r = 7.9$ and 7.7 systems, the P versus the bias voltage across the FE layer (V_f) exhibits a negative slope. On the other hand, the stack capacitor with
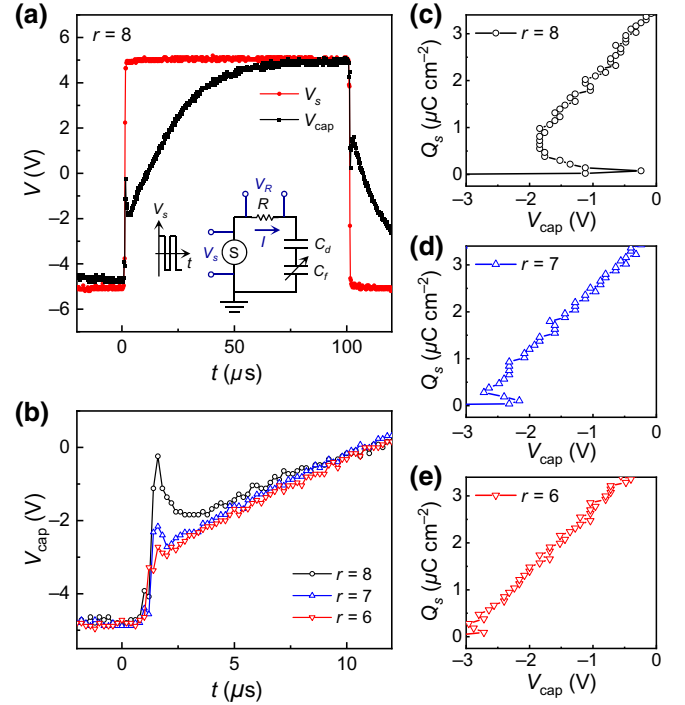
$r = 7.9$ still exhibits clear switching hysteresis [Fig. 3(c)], while hysteresis becomes absent in the system with $r = 7.7$ [Fig. 3(d)].

IV. TRANSIENT NEGATIVE-CAPACITANCE STATE

The evolution of energy profile can be further probed by assessing the charge-switching dynamics in the stack capacitors. The existence of a negative curvature at zero bias voltage is manifested as a transient NC behavior during polarization switching [4]. As shown in Fig. 4(a) inset, we apply a square voltage wave to the stack capacitor, which is connected in series with a load resistor of 9.86 kΩ. The source voltage V_s and the voltage drop across the load resistor V_R are measured simultaneously, based on which we deduce the voltage across the stack capacitor $V_{cap} = V_s - V_R$ (Supplemental Material) [24]. Figure 4(a) shows one charging-discharging cycle of V_s and V_{cap} for the $r = 8$ sample. The voltage on the capacitor is initially saturated, suggesting that the sample is fully polarized in a single domain state. Upon the voltage switching to positive, we observe a sharp drop in V_{cap} after initial rise. The damping process lasts about 2 μs, after which the system restores the typical charging behavior of a capacitor.

We then characterize the charge-switching dynamics of stack capacitors with different r. As shown in Fig. 4(b), the charge damping magnitude is significantly suppressed in the $r = 7$ sample, and becomes barely recognizable in the $r = 6$ sample. This observation is in excellent agreement with the P-E results, which shows the ferroelectric order is quenched at a $r = 8$–7 [Fig. 2(c)]. When the stack capacitors transition from the FE phase to DE phase with decreasing r, the free energy evolves from the double-well structure to a single minimal [Fig. 3(b)], while the damping of voltage originating from the NC region becomes absent in the latter case. The existence of transient NC effect is directly reflected in the V dependence of the free charge density Q_s on the PZT/STO stack capacitor [6,8]. For each V_{cap} value, we extract the corresponding Q_s by integrating the charging or discharging current $I = V_R/R$ with respect to time [Fig. 4(a) inset] upon one cycle of the square wave of V_s. As shown in Figs. 4(c)–4(e), for the $r = 8$ sample, Q_s-V_{cap} shows a clear S-shape upon initial polarization switching, only resuming a positive slope after Q_s reaches about $0.8\,\mu\text{C}\,\text{cm}^{-2}$. The S-feature becomes less prominent in the $r = 7$ sample, and basically disappears in the $r = 6$ sample, indicating that the system is gradually dominated by the dielectric behavior.

V. MODELING OF VOLTAGE DAMPING IN THE TRANSIENT NC STATE

To gain a quantitative understanding of the voltage damping during the transient NC process, we consider the charging dynamics of a RC in series circuit:

$$\frac{\partial Q_{\text{free}}}{\partial t} = \frac{V_s - V_{\text{cap}}}{RA}, \tag{3}$$

$$Q_{\text{free}} = \varepsilon_0 E_{\text{ext}} + P, \tag{4}$$

where Q_{free} is the free charge density, P is the apparent polarization of the capacitor, and $E_{\text{ext}} = V_{\text{cap}}/(t_d + t_f)$. The transient NC effect can be treated as resulting from the mismatch between the instantaneous polarization and charge screening. We consider several models describing the relation between E_{ext} and P. The Landau-Khalatnikov (LK) dissipative model [2,33,34] assumes a single-domain scenario, where polarization is switched uniformly. When the FE/DE stack goes through the depoled state ($P = 0$), the negative curvature of the free-energy profile is manifested as a negative differential capacitance, which leads to a voltage damping in the presence of the increasing driving voltage. The capacitor voltage under nonequilibrium condition can be expressed as

$$E_{\text{ext}} = \frac{1}{t_d + t_f}\frac{\partial g_0}{\partial P} + \rho\frac{dP}{dt}, \tag{5}$$
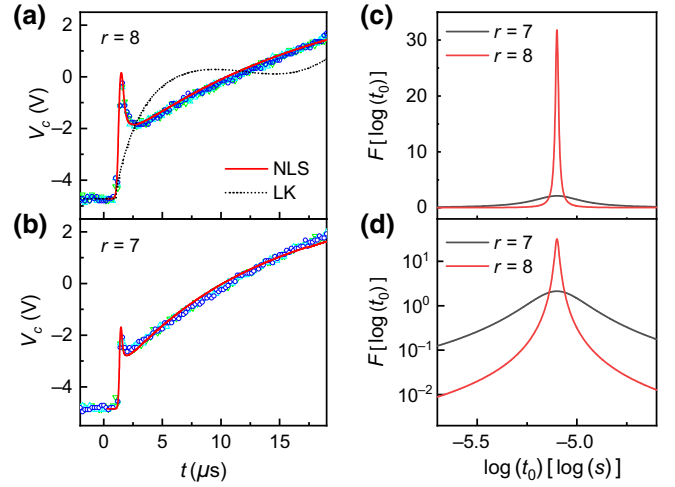

FIG. 5. (a),(b) Three sets of $V_c(t)$ data in the transient NC regime (open symbols) for the (a) $r = 8$ and (b) $r = 7$ samples with fits to the KAI/NLS model (solid line) and LK model (dashed line). (c),(d) Distribution functions of $\log(t_0)$ extracted from the NLS fitting results for the $r = 8$ (red) and $r = 7$ (black) samples plotted on (c) linear and (d) logarithmic scales.

where g_0 is the free energy areal density at zero bias, and ρ is the viscosity coefficient. Adopting Eq. (1) for the free-energy term, we derive the LK dissipative formula for the uniform polarization switching dynamics as

$$E_{\text{ext}} = \rho\frac{dP}{dt} + \frac{r}{1 + r}(2\alpha P + 4\beta P^3 + 6\gamma P^5)$$
$$+ \frac{1}{1 + r} \times \frac{P}{\varepsilon_d \varepsilon_0}. \tag{6}$$

Assuming that the stack is initially fully polarized, we can solve for the charge dynamics upon polarization switching. In Fig. 5(a), we plot the simulated result for the $r = 8$ sample based on the LK model. While the model does predict a charge-damping phenomenon, the fit deviates significantly from the experimental data. The uniform polarization switching model cannot fully capture the observed transient NC behavior as it does not take domain formation into account [18,22].

To correctly model the charge-switching dynamics, we need to consider two additional processes that are energetically more preferable than the uniform switching scenario in the FE/DE stack capacitors [22]. First, for the FE behavior dominated region with thick FE layers, the polarization switching follows the NG process. Second, as the fraction of STO becomes sufficiently high, the system prefers the multidomain state due to the presence of high depolarization field [10,11,23].

For the NG-dominated regime, the polarization reversal initially occurs at a few small sites due to defects or fluctuation (nucleation). The domain then expands under the external field (growth) through DW motion. During

the domain growth process, the ferroelectric remains in a polarized state everywhere except for the DW regions. It thus maintains a much smaller global energy compared with the uniform switching process, which requires the entire material going through the double-well energy barrier simultaneously. By considering a freely moving DW model, the change in the apparent polarization during the growth process can be described statistically as $\Delta P \propto 1 - \exp[-(t/t_0)^n]$, known as the Kolmogorov-Avrami-Ishinashi (KAI) factor [35–38]. Here n is the effective dimensionality of the system, and t_0 is the characteristic switching time determined by the growth of reversed domains generated from the nucleation. In this scenario, the apparent voltage damping can be phenomenologically explained as the mismatch between bound charge and free charge.

The KAI model has been generalized to ferroelectric thin films by considering the competition between nucleation and DW motion [15–17,19], as the latter is also limited by defect pinning and size confinement. In this scenario, the film can be considered as consisting of multiple independent switching areas, with t_0 described by a distribution function. Tagantsev *et al.* developed a nucleation-limited-switching (NLS) model by replacing t_0 with a statistical average form [15]. Due to the nature of dipole-dipole interaction between different nucleation regions, Jo *et al.* proposed a Lorentzian distribution of $\log(t_0)$ [16], which yields

$$\Delta P(t) = 2P_r \int_{-\infty}^{+\infty} d(\log t_0)$$
$$\left\{ 1 - \exp\left[-\left(\frac{t}{t_0}\right)^n \right] \right\} F(\log t_0), \qquad (7)$$

where

$$F(\log t_0) = \frac{1}{\pi} \frac{w}{(\log t_0 - \log t_1)^2 - w^2}$$

describes the Lorentzian distribution of t_0 centered at t_1 with HWHM of w. Here t_0 is proportional to the distance between different nucleation regions divided by the DW velocity. Using the DW creep model: $v \propto \exp[-(U/k_B T)(E_0/E_f)]$, with U the energy barrier and E_0 the threshold field, the associated distribution parameters can be expressed as $\log(t_1) \propto 1/E_{\text{creep}}$ and $w \propto 1/E_{\text{creep}}^2$ [16]. Here E_{creep} represents the effective field contributing to DW creep, which serves as an intermediate parameter in our modeling. The NG model usually corresponds to a much faster apparent switching rate [22].

For samples with reduced layer thickness or close to the FE-DE transition regime, the enhanced depolarization field gradually dominates the free-energy profile, which can lead to the formation of a multidomain state [10,11,39]. In this scenario, the domain formation occurs ahead of the domain expansion. The apparent polarization is thus a result of the net difference between the domain fractions of opposite polarizations, which is much smaller than the spontaneous polarization within a domain. In the multidomain state, the DW density is much higher than the NG scenario. The DW becomes soft and less mobile, and the slower DW motion results in much slower polarization switching than in the NG case [22]. This scenario can account for the shoulder feature observed in the *P-E* hysteresis [Fig. 2(a)] and the emergence of steady-state NC effect at small *r* [Fig. 2(b)].

In Figs. 5(a) and 5(b), we fit the transient regime using the combination of the NG and LK models with three sets of $V_{\text{cap}}(t)$ data taken on the $r = 8$ and 7 samples. We modify Eq. (7) by defining $E_{\text{creep}} = E_{\text{ext}} - a E_{\text{LGD}}$, where $E_{\text{LGD}} = V/(t_f + t_d)$ is calculated from Eq. (2) using the apparent polarization of the system, and a is a fitting parameter. In the transient NC regime, E_{creep} embeds the competing effects of ferroelectric ordering energy, depolarization, domain formation, and the presence of DWs, and can only be obtained by minimizing the total free energy. This model gives rise to an excellent description of the measured $V_{\text{cap}}(t)$ in the transient NC regime, with the fitting parameters given in Table S2 within the Supplemental Material [24]. The fit to the $r = 7$ system requires a higher correction associated with the LGD field, which reflects the modified energy landscape in the multidomain state at high STO content.

Figures 5(c) and 5(d) show the distribution functions we adopt for the fits to the initial switching, i.e., $V_{\text{cap}} = V_s$. For the $r = 8$ sample, we start from a fully polarized state, with the initial polarization settled at the measured P_r (approximately $53\,\mu\text{C cm}^{-2}$) [Fig. 2(c)]. The distribution function of $\log(t_0)$ shows a very narrow Lorentzian function, with the HWHM orders of magnitude narrower than those observed in polycrystalline PZT [16]. This result indicates that the polarization switching at large *r* is highly homogenous, and the occurrences of nucleation are almost simultaneous. We consider the initial nucleation occurs at the interfacial defect sites, with the DW motion along the electric field direction [40,41]. The narrow distribution of switching time thus confirms the high crystalline quality of our samples. For the $r = 7$ sample, we use an initial simulated polarization ($28\,\mu\text{C cm}^{-2}$), which is comparable with the experimental remnant polarization ($25\,\mu\text{C cm}^{-2}$). The $\log(t_0)$ for $r = 7$ shows a significantly broadened distribution, indicating a nucleation-dominated switching. This observation can be attributed to the formation of nanoscale bubble domains or multidomain state [42]. In this scenario, the nucleation sites are no longer concentrated at the interface and can locate within the film, where the emergence of the domain structure modifies the local energy landscape, leading to a broadening of characteristic switching time. In addition, the DW motion is impeded by the quasistatic,

soft DWs [10], leading to reduced mismatch between polarization and charge screening and thus suppressed the damping effect for V_{cap}.

VI. CONCLUSION

In summary, we report a comprehensive study of *P-V*, *C-V*, charge-switching dynamics in high-quality epitaxial PZT/STO stack capacitors with different thickness ratios. The transition from the ferroelectric to dielectric dominated behavior occurs at a critical ratio of 8–7, which agrees with Landau theory modeling assuming a single-domain picture. Close to the critical ratio, the transient NC polarization switching in the ferroelectriclike PZT/STO stack can be well described by the nucleation and growth-dominated behavior with an extremely narrow distribution of the characteristic switching time. A broadening of the switching time is observed at slightly higher STO content, which is attributed to the emergence of the multidomain state. Our study sheds light on the effects of materials parameters and domain formation on the ferroelectric-dielectric transition in these hybrid systems, which facilitates the design of the steady-state NC mode for developing steep-slope transistor with hysteresis-free operation.

[1] S. Salahuddin and S. Datta, Use of negative capacitance to provide voltage amplification for low power nanoscale devices, Nano Lett. **8**, 405 (2008).

[2] J. Íñiguez, P. Zubko, I. Luk'yanchuk, and A. Cano, Ferroelectric negative capacitance, Nat. Rev. Mater. **4**, 243 (2019).

[3] M. M. Waldrop, The chips are down for Moore's law, Nature **530**, 144 (2016).

[4] S.-C. Chang, U. E. Avci, D. E. Nikonov, S. Manipatruni, and I. A. Young, Physical Origin of Transient Negative Capacitance in a Ferroelectric Capacitor, Phys. Rev. Appl. **9**, 014010 (2018).

[5] K. Majumdar, S. Datta, and S. P. Rao, Revisiting the theory of ferroelectric negative capacitance, IEEE Trans. Electron Devices **63**, 2043 (2016).

[6] A. I. Khan, K. Chatterjee, B. Wang, S. Drapcho, L. You, C. Serrao, S. R. Bakaul, R. Ramesh, and S. Salahuddin, Negative capacitance in a ferroelectric capacitor, Nat. Mater. **14**, 182 (2015).

[7] M. Hoffmann, A. I. Khan, C. Serrao, Z. Lu, S. Salahuddin, M. Pešić, S. Slesazeck, U. Schroeder, and T. Mikolajick, Ferroelectric negative capacitance domain dynamics, J. Appl. Phys. **123**, 184101 (2018).

[8] M. Hoffmann, F. P. G. Fengler, M. Herzig, T. Mittmann, B. Max, U. Schroeder, R. Negrea, P. Lucian, S. Slesazeck, and T. Mikolajick, Unveiling the double-well energy landscape in a ferroelectric layer, Nature **565**, 464 (2019).

[9] H. Ryu, K. Xu, D. Li, X. Hong, and W. Zhu, Empowering 2D nanoelectronics via ferroelectricity, Appl. Phys. Lett. **117**, 080503 (2020).

[10] P. Zubko, J. C. Wojdel, M. Hadjimichael, S. Fernandez-Pena, A. Sene, I. Luk'yanchuk, J. M. Triscone, and J. Iniguez, Negative capacitance in multidomain ferroelectric superlattices, Nature **534**, 524 (2016).

[11] A. K. Yadav, K. X. Nguyen, Z. J. Hong, P. Garcia-Fernandez, P. Aguado-Puente, C. T. Nelson, S. Das, B. Prasad, D. Kwon, S. Cheema, A. I. Khan, C. M. Hu, J. Iniguez, J. Junquera, L. Q. Chen, D. A. Muller, R. Ramesh, and S. Salahuddin, Spatially resolved steady-state negative capacitance, Nature **565**, 468 (2019).

[12] A. I. Khan, D. Bhowmik, P. Yu, S. J. Kim, X. Pan, R. Ramesh, and S. Salahuddin, Experimental evidence of ferroelectric negative capacitance in nanoscale heterostructures, Appl. Phys. Lett. **99**, 113501 (2011).

[13] X. Chen, X. Zhang, M. A. Koten, H. Chen, Z. Xiao, L. Zhang, J. E. Shield, P. A. Dowben, and X. Hong, Interfacial charge engineering in ferroelectric-controlled Mott transistors, Adv. Mater. **29**, 1701385 (2017).

[14] A. Cano and D. Jiménez, Multidomain ferroelectricity as a limiting factor for voltage amplification in ferroelectric field-effect transistors, Appl. Phys. Lett. **97**, 133509 (2010).

[15] A. K. Tagantsev, I. Stolichnov, N. Setter, J. S. Cross, and M. Tsukada, Non-Kolmogorov-Avrami switching kinetics in ferroelectric thin films, Phys. Rev. B **66**, 214109 (2002).

[16] J. Y. Jo, H. S. Han, J. G. Yoon, T. K. Song, S. H. Kim, and T. W. Noh, Domain Switching Kinetics in Disordered Ferroelectric Thin Films, Phys. Rev. Lett. **99**, 267602 (2007).

[17] N. Gong, X. Sun, H. Jiang, K. S. Chang-Liao, Q. Xia, and T. P. Ma, Nucleation limited switching (NLS) model for HfO_2-based metal-ferroelectric-metal (MFM) capacitors: Switching kinetics and retention characteristics, Appl. Phys. Lett. **112**, 262903 (2018).

[18] Y. J. Kim, H. W. Park, S. D. Hyun, H. J. Kim, K. D. Kim, Y. H. Lee, T. Moon, Y. B. Lee, M. H. Park, and C. S. Hwang, Voltage drop in a ferroelectric single layer capacitor by retarded domain nucleation, Nano Lett. **17**, 7796 (2017).

[19] A. Gruverman, B. J. Rodriguez, C. Dehoff, J. D. Waldrep, A. I. Kingon, R. J. Nemanich, and J. S. Cross, Direct studies of domain switching dynamics in thin film ferroelectric capacitors, Appl. Phys. Lett. **87**, 082902 (2005).

[20] A. M. Bratkovsky and A. P. Levanyuk, Abrupt Appearance of the Domain Pattern and Fatigue of Thin Ferroelectric Films, Phys. Rev. Lett. **84**, 3177 (2000).

[21] A. M. Bratkovsky and A. P. Levanyuk, Very large dielectric response of thin ferroelectric films with the dead layers, Phys. Rev. B **63**, 132103 (2001).

[22] H. W. Park, J. Roh, Y. B. Lee, and C. S. Hwang, Modeling of negative capacitance in ferroelectric thin films, Adv. Mater. **31**, 1805266 (2019).

[23] M. Hoffmann, M. Pešić, S. Slesazeck, U. Schroeder, and T. Mikolajick, On the stabilization of ferroelectric negative capacitance in nanoscale devices, Nanoscale **10**, 10891 (2018).

[24] See Supplemental Material at http://link.aps.org/supplemental/10.1103/PhysRevApplied.16.034004 for additional details of sample growth, characterization, and data modeling.

[25] K. Wang, Y. Hao, L. Zhang, Y. Zhang, X. Chen, and X. Hong, Effect of correlated oxide electrodes on disorder pinning and thermal roughening of ferroelectric domain walls in epitaxial $PbZr_{0.2}Ti_{0.8}O_3$ thin films, Phys. Rev. Mater. **5**, 074402 (2021).

[26] L. C. Tănase, L. E. Abramiuc, D. G. Popescu, A.-M. Trandafir, N. G. Apostol, I. C. Bucur, L. Hrib, L. Pintilie, I. Pasuk, L. Trupină, and C. Teodorescu, Polarization Orientation in Lead Zirconate Titanate (001) Thin Films Driven by the Interface with the Substrate, Phys. Rev. Appl. **10**, 034020 (2018).

[27] H. W. Jang, A. Kumar, S. Denev, M. D. Biegalski, P. Maksymovych, C. W. Bark, C. T. Nelson, C. M. Folkman, S. H. Baek, N. Balke, C. M. Brooks, D. A. Tenne, D. G. Schlom, L. Q. Chen, X. Q. Pan, S. V. Kalinin, V. Gopalan, and C. B. Eom, Ferroelectricity in Strain-Free $SrTiO_3$ Thin Films, Phys. Rev. Lett. **104**, 197601 (2010).

[28] Y. S. Kim, D. J. Kim, T. H. Kim, T. W. Noh, J. S. Choi, B. H. Park, and J.-G. Yoon, Observation of room-temperature ferroelectricity in tetragonal strontium titanate thin films on $SrTiO_3$ (001) substrates, Appl. Phys. Lett. **91**, 042908 (2007).

[29] D. Lee, H. Lu, Y. Gu, S.-Y. Choi, S.-D. Li, S. Ryu, T. R. Paudel, K. Song, E. Mikheev, S. Lee, S. Stemmer, D. A. Tenne, S. H. Oh, E. Y. Tsymbal, X. Wu, L.-Q. Chen, A. Gruverman, and C. B. Eom, Emergence of room-temperature ferroelectricity at reduced dimensions, Science **349**, 1314 (2015).

[30] D. Fuchs, C. W. Schneider, R. Schneider, and H. Rietschel, High dielectric constant and tunability of epitaxial $SrTiO_3$ thin film capacitors, J. Appl. Phys. **85**, 7362 (1999).

[31] J. Kim, L. Kim, D. Jung, I. W. Kim, J. H. Je, and J. Lee, Effect of oxygen cooling environment on the structural characteristics and dielectric properties of $BaTiO_3$ and $SrTiO_3$ thin films, Ferroelectrics **327**, 103 (2005).

[32] Y. W. So, D. J. Kim, T. W. Noh, J.-G. Yoon, and T. K. Song, Polarization switching kinetics of epitaxial $Pb(Zr_{0.4}Ti_{0.6})O_3$ thin films, Appl. Phys. Lett. **86**, 092905 (2005).

[33] L. D. Landau and I. M. Khalatnikov, On the anomalous absorption of sound near a second order phase transition point, Dokl. Akad. Nauk SSSR **96**, 469 (1954).

[34] S. Sivasubramanian, A. Widom, and Y. N. Srivastava, Physical kinetics of ferroelectric hysteresis, Ferroelectrics **300**, 43 (2004).

[35] M. Avrami, Kinetics of phase change. II transformation-time relations for random distribution of nuclei, J. Chem. Phys. **8**, 212 (1940).

[36] A. N. Kolmogorov, On the statistical theory of crystallization of metals, Izv. Akad. Nauk SSSR, Ser. Mat. **3**, 355 (1937).

[37] H. Orihara, S. Hashimoto, and Y. Ishibashi, A theory of D-E hysteresis loop based on the avrami model, J. Phys. Soc. Jpn. **63**, 1031 (1994).

[38] in *Ferroelectric Thin Films: Synthesis and Basic Properties*, edited by C. P. De Araujo, J. F. Scott, G. W. Taylor (Gordon and Breach Publishers, Amsterdam, The Netherlands, 1996).

[39] A. M. Bratkovsky and A. P. Levanyuk, Depolarizing field and "real" hysteresis loops in nanometer-scale ferroelectric films, Appl. Phys. Lett. **89**, 253108 (2006).

[40] M.-G. Han, M. S. J. Marshall, L. Wu, M. A. Schofield, T. Aoki, R. Twesten, J. Hoffman, F. J. Walker, C. H. Ahn, and Y. Zhu, Interface-induced nonswitchable domains in ferroelectric thin films, Nat. Commun. **5**, 4693 (2014).

[41] P. Hou, J. Wang, X. Zhong, and Y. Wu, A ferroelectric memristor based on the migration of oxygen vacancies, RSC Adv. **6**, 54113 (2016).

[42] Q. Zhang, L. Xie, G. Liu, S. Prokhorenko, Y. Nahas, X. Pan, L. Bellaiche, A. Gruverman, and N. Valanoor, Nanoscale bubble domains and topological transitions in ultrathin ferroelectric films, Adv. Mater. **29**, 1702375 (2017).